IEEE Access
Multidisciplinary | Rapid Review | Open Access Journal

Received April 3, 2019, accepted May 18, 2019, date of publication May 29, 2019, date of current version June 11, 2019.

Digital Object Identifier 10.1109/ACCESS.2019.2919451

Optimization of Surgical Illuminant Spectra for Organ Microstructure Visualization

YOKO KURABUCHI[1], KAZUYA NAKANO[2], TAKASHI OHNISHI[2], TOSHIYA NAKAGUCHI[2], MARKKU HAUTA-KASARI[3], AND HIDEAKI HANEISHI[2]

[1]Graduate School of Science and Engineering, Chiba University, Chiba 263-8522, Japan
[2]Center for Frontier Medical Engineering, Chiba University, Chiba 263-8522, Japan
[3]School of Computing, University of Eastern Finland, FI-80101 Joensuu, Finland

Corresponding author: Yoko Kurabuchi (y_kurabuchi@chiba-u.jp)

This work was supported in part by the KAKENHI under the Grant-in-Aid for Scientific Research (A) Grant number 16H01855, and in part by the JSPS Core-to-Core Program.

ABSTRACT In a delicate operation, the appearance of organs and tissues is an essential factor for surgeons to figure out the hemodynamic state of the tissue or identify vascular regions. In open surgery, surgeons have a direct view of the surgical area with the naked eye or through a microscope. Under these circumstances, the spectral characteristics of a surgical illuminant are the most effective factor to ensure successful operations. In this study, we designed an optimal surgical illuminant to enhance microvascular structures. Two factors were used in the design: illuminant whiteness and the contrast between tissues and blood vessels. We subsequently prototyped a tunable light source using 14 types of light-emitting diodes (LEDs) with different spectral radiances to reproduce the illuminant spectra of the designed and conventional surgical illuminant. Using this light source, we conducted subjective evaluation experiments with three rat ceca whose detected vessel regions were measured with a conventional and optimal illuminant. We confirmed that the optimal illuminant was significantly superior to the conventional illuminant to view fine vascular structures.

INDEX TERMS Light emitting diodes, lighting, surgical instruments, microstructure, color appearance.

I. INTRODUCTION

In a delicate operation, successful surgery requires the precise skills of a surgeon. Visual diagnoses are particularly important to evaluate the situation in an operation area. The color and structures of organs and tissues are essential to understand blood circulation and disease conditions. In endoscopic diagnosis and laparoscopic surgery, an electric camera is used to obtain images of the organs. Thus, the camera itself is important for providing sufficient information to surgeons. For example, narrow-band imaging is widely used to visualize detailed structures in vascular patterns [1] for endoscopic diagnosis. Meanwhile, in an open surgery, when surgeons view the surgical area directly with the naked eye or through a microscope, the illuminant is the most effective factor that supports a surgeons' direct observation. In particular, the spectral characteristics of the surgical illuminant can potentially improve the appearance of the surgical area.

The associate editor coordinating the review of this manuscript and approving it for publication was Rajeswari Sundararajan.

Optimal surgical illuminants have been designed previously using computer simulation [2]–[8]. Next, prototyping the designed illuminant and its evaluation is essential for practical use. In [9], [10], the authors optimized the spectra of light-emitting diodes (LEDs) and implemented an LED ceiling system. The authors optimized surgical illuminants by contrast enhancement based on entropy analysis. In [11], the authors optimized illuminants to improve visualization of retinal images using a spectrally tunable light source based on a digital micromirror device.

We previously reported an optimal illuminant that yielded clearer views of blood circulation [12]. The illuminant was designed to enhance the color differences between ischemic and normal tissues. We developed the optimal illuminant using a spectrally tunable light source and performed animal experiments. We confirmed the effectiveness of the illuminant to enhance ischemic tissue. Furthermore, through evaluation experiments, we discovered that observing blood vessel structures for hemodynamic monitoring was another important factor during surgery. Especially in microsurgery, fine structures in the surgical field are viewed through a

surgical microscope. In such cases, since surgeons use an optical system to perform observation, the illuminant spectra are important and can be further improved to enhance blood vessel structures.

Thus, we aimed to design a different type of optimal surgical illuminant that can enhance microvascular structures. We designed optimal illuminant spectra to satisfy two requirements. Surgeons operate with a conventional shadowless illuminant in an operation room. Extreme changes in illumination from the conventional illuminant may cause confusion. Therefore, illuminant whiteness was the first factor in optimization. Here illuminant whiteness was defined based on the appearance of a white object identical to that when using a conventional illuminant. The second factor was the contrast between tissues and blood vessels. We maximized a gray-level contrast between the two areas. For illuminant optimization, we maximized the contrast between the two areas, so that we could yielded a sufficiently small color difference between the optimized illuminant and a conventional illuminant. We defined this illuminant as the white-color-preserving emphatic illuminant hereinafter referred to as WCPEI.

For comparison, a conventional illuminant spectrum was mimicked using the prototype tunable light source. The mimicked conventional illuminant was defined as a spectrally-tuned conventional illuminant hereinafter referred to as STCI. Then we conducted an evaluation experiment using our prototype tunable light source to reproduce the WCPEI and the STCI spectra. We conducted a subjective evaluation experiment with rat ceca and evaluated WCPEI effectiveness. Participants observed the microvascular structure under the two illuminant conditions, the WCPEI and the STCI. We compared the blood vessel regions detected by the observers under the two illuminant conditions and confirmed WCPEI effectiveness.

II. METHOD OF SPECTRAL DISTRIBUTION OPTIMIZATION

We generated the WCPEI by combining LED spectra. An optimized spectrum, $E_{\mathrm{op}}(\lambda)$, is defined as follows:

$$E_{\mathrm{op}}(\lambda) = \sum_n w_n E_n(\lambda) \quad 0 \le w_n \le 1,\ n = 1, \cdots, N \tag{1}$$

where N is the number of LEDs, $E_n(\lambda), n = 1, \ldots, N$, denotes the normalized spectral radiation for each LED, w_n denotes the weight for the nth LED that ranges from 0 to 1. In the optimization, the weights $\{w_n\}$ are the parameters that we aim to optimize. The spectral energy of the reflected light is given by $E_{\mathrm{op}}(\lambda) R(\lambda)$, where $R(\lambda)$ denotes the spectral reflectance of a reflective object. The color perceived by a standard human observer is modeled by tristimulus values, X, Y, and Z, by combining $\bar{x}(\lambda)$, $\bar{y}(\lambda)$, and $\bar{z}(\lambda)$, i.e., the color-matching functions related to spectral sensitivity of cones in the retina defined by the International Commission on Illumination (CIE). We used the color appearance model, CIECAM02, to calculate the color difference, $\Delta E'$, and contrast value as an evaluation index to obtain the contrast between tissue and blood vessels [13].

As mentioned earlier, the WCPEI must exhibit the two predefined conditions: (1) it enhances blood vessel structures and (2) it provides an identical appearance of the perfect diffuser (white object) to the conventional illuminant. For comparison, Skylux Crystal (Yamada Shadowless Lamp Co., Ltd.) was used for the conventional illuminant reference. The contrast value, α, was calculated using the Michelson contrast [14]. To evaluate the contrast between tissues and blood vessels with the WCPEI, we calculated the following contrast using the calculated lightness value, J', which is reformed from the lightness value, J, based on the CIECAM02 model [13], as follows:

$$\alpha = \frac{\max\left|J'_{\mathrm{tis}}, J'_{\mathrm{ves}}\right| - \min\left|J'_{\mathrm{tis}}, J'_{\mathrm{ves}}\right|}{J'_{\mathrm{tis}} + J'_{\mathrm{ves}}} \tag{2}$$

where J'_{tis} and J'_{ves} represent the lightness values of the tissue and blood vessels, respectively. These values, J'_{tis} and J'_{ves}, are calculated from the measured spectral reflectance of the tissue, $R_{\mathrm{tis}}(\lambda)$, and blood vessels, $R_{\mathrm{ves}}(\lambda)$, respectively.

The whiteness of the WCPEI was evaluated with β, the color differences of a perfect diffuser regarding the two illuminant conditions, i.e., the conventional illuminant, $E_{\mathrm{con}}(\lambda)$, and the WCPEI. We calculated the color difference between the two illuminant colors defined by CIECAM02 as follows:

$$\beta = \left(\left(\Delta J'/K_L\right)^2 + \left(\Delta a'_M\right)^2 + \left(\Delta b'_M\right)^2\right)^{1/2} \tag{3}$$

where $\Delta J'$ represents the difference between J'_{con} and J'_{op}, $\Delta a'_M$ and $\Delta b'_M$ represent the Cartesian coordinate difference between two chromatic factors, $a'_{M\mathrm{con}}$, $a'_{M_{\mathrm{op}}}$ and $b'_{M\mathrm{con}}$, $b'_{M_{\mathrm{op}}}$, respectively. A combination of $\Delta a'_M$ and $\Delta b'_M$ represents a chromaticity difference between the conventional illuminant and the WCPEI. These values are calculated from the illuminant spectra, $E_{\mathrm{con}}(\lambda)$ and $E_{\mathrm{op}}(\lambda)$. K_L denotes the parameter for the coefficient value, which was set as $K_L = 1.0$. To satisfy the requirements mentioned above, we sought a WCPEI that maximized α under the condition that β was less than 3.0. The color difference of 3.0 is regarded as a perceivable limit. Fig. 1 shows the flowchart of illumination optimization. Through this optimization flow, we established both LED selection and intensity setting at the same time. Particle swarm optimization was used as an optimization method [15]. For each iteration step, we updated the best local and global α if the weights $\{w_n\}$ satisfied the limitation of $\beta < 3.0$.

III. EXPERIMENTS

A. EMPHATIC DESIGN OF ILLUMINANT SPECTRA

1) DATA COLLECTION OF TISSUE AND BLOOD VESSELS FOR ILLUMINANT DESIGN

Rat cecum was used in this experiment for preclinical tests in advance of human participants. First, we captured image

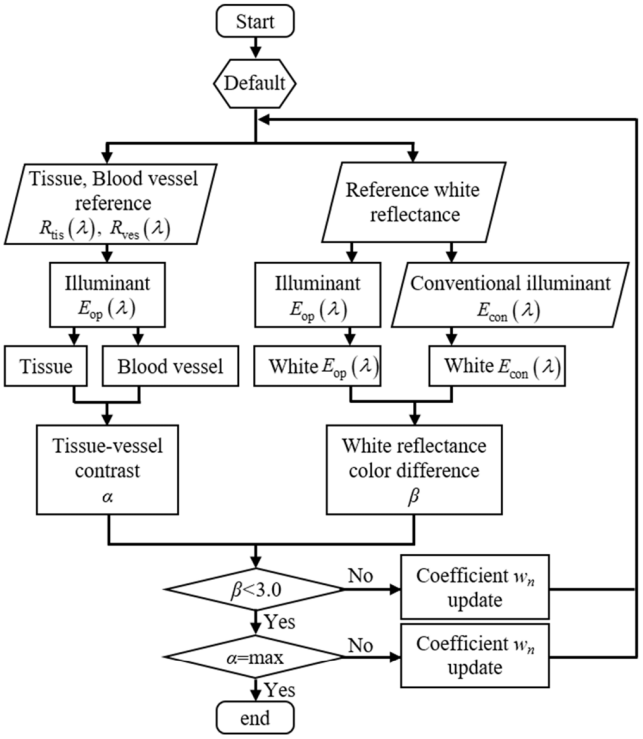

FIGURE 1. Flowchart of illumination optimization.

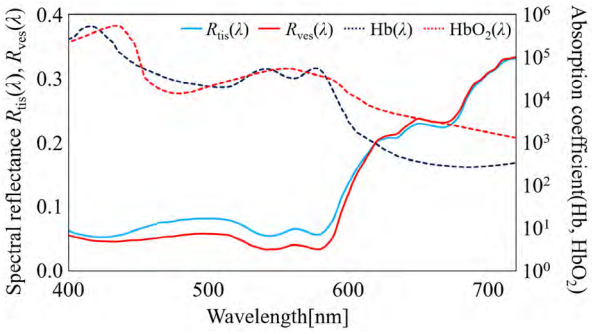

FIGURE 2. Spectral reflectance of organ tissue and blood vessels (solid lines) and the spectral absorption of Hb and HbO_2 (dashed lines).

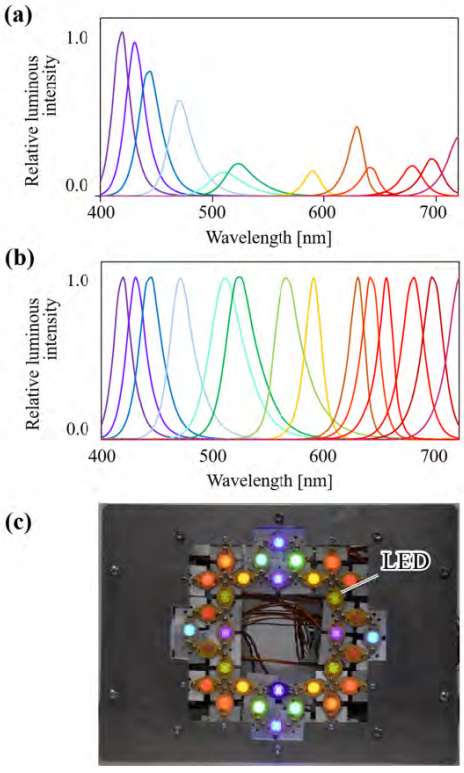

FIGURE 3. Spectrally tunable light source. (a) Measured spectra of each LED. (b) Normalized spectral LED distributions. (c) Light source unit of the spectrally tunable light source.

sets of the rat cecum with a hyperspectral camera and calculated the spectral reflectance. The camera used was NH-8 (EBA Japan Co., Ltd.), which has 1,200 × 1,024 pixels, 12 bits per pixel, and covers a range in wavelength from 380 to 1,000 nm with 5 nm intervals. Its image capturing geometry was based on the CIE recommendation [16]. Xenon light was illuminated normal to the target and images were captured from a direction of 45° . The rat cecum was pulled out from the abdomen and affixed to a jig without blocking blood flow under anesthesia. A rat body was placed on an electric carpet (temperature: 38 ± 2 °C) to maintain a stable body temperature. We monitored the rat's heart rate and oxygen saturation as vital signs throughout the experiment. As an illuminant spectrum reference, images of a perfect standard reflector were captured under identical imaging geometry to calculate sample spectral reflectance. The spectral reflectance of the two target regions, i.e., organ tissue surface and blood vessels, (R_{tis} (λ) and R_{ves} (λ)), were calculated from a set of hyperspectral images. This measurement and the evaluation experiment mentioned later were performed in conformity with the Institutional Animal Care and Use Policy of Chiba University.

Fig. 2 shows the results of spectral reflectance, i.e., R_{tis} (λ) and R_{ves} (λ). The blood vessel reflectance, R_{ves} (λ), exhibits a lower reflectance value between 400 and 600 nm compared with the tissue reflectance, R_{tis} (λ). The difference is possibly caused by the hemoglobin content, which is a dominant absorber in a living organism in the visible range. The hemoglobin concentration in blood vessels is thought to be higher than that in the tissue region. This leads to lower R_{ves} (λ) values in the shorter wavelength region.

2) PROTOTYPING SPECTRALLY TUNABLE LIGHT SOURCE

To reproduce the illuminant spectra of the WCPEI and the STCI by applying (1), we prototyped a spectrally tunable light source with 14 commercially available high-intensity LEDs (Ushio Epitex Inc.) based on our previous device [12].

The peak wavelengths of the 14 types of LED were 420, 430, 450, 470, 505, 525, 565, 590, 630, 645, 660, 680, 700, and 720 nm, which covered the entire visible range. Fig. 3 shows spectral characteristics and a picture of the light source. We measured the spectral intensities of the LEDs

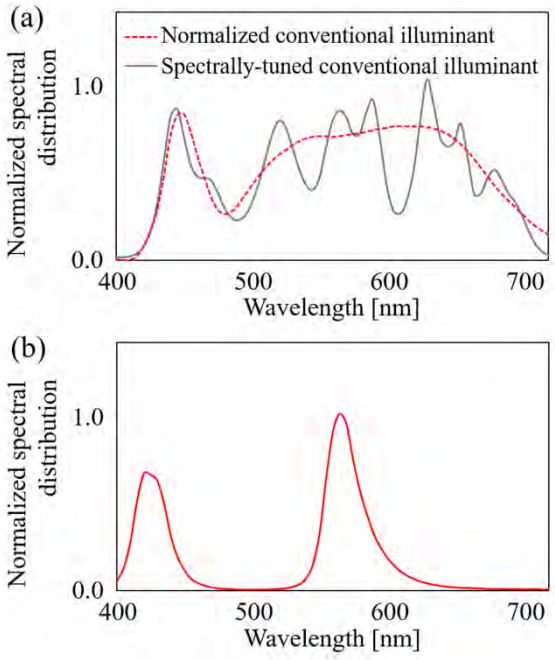

FIGURE 4. Illuminant spectra. (a) Conventional illuminant. (b) The WCPEI.

using a spectral radiance meter, SR-LEDW (Topcon Co.), for WCPEI spectrum simulation. Fig. 3(a) shows the measured spectral distributions of each LED at the same electric current. For each wavelength, two units were mounted. However, for the two types of low-intensity LEDs with peak wavelengths at 565 nm and 590 nm, four units were mounted to diminish intensity variations in each LED. Figure 3(b) shows the intensity-normalized spectra by each peak intensity, $E_n(\lambda) = 1, 2, \cdots, 14$, and Fig. 3(c) shows a picture of the LED units that comprise the spectrally tunable light source. The simulated illuminant spectra were reproduced by pulse width modulation. Using this method, we set intensities of each LED after normalizing the intensity variation between the LEDs. In this experiment, we defined the operation field by a square of 20 cm $\times$ 20 cm right below the prototype light source and confirmed the spatial uniformity of spectra in the operating field before the evaluation experiment.

3) WHITE-COLOR-PRESERVING EMPHATIC ILLUMINANT DESIGN

The dotted line in Fig. 4(a) shows the illuminant spectrum used for the whiteness condition, Skylux Crystal (Yamada Shadowless Lamp Co., Ltd.). In the experiment, we mimicked this spectrum, shown by the solid line in Fig. 4(a).

Fig. 4(b) shows the calculated WCPEI spectrum. The calculated spectrum contains two peaks at approximately 565 and 420 nm. These two peaks were located especially high in the absorption range of Hb and HbO_2. Additionally, the calculated spectrum exhibited power in the 600 nm range or shorter, matching with the range in which the spectral reflectance, $R_{tis}(\lambda)$ and $R_{ves}(\lambda)$, had large differences.

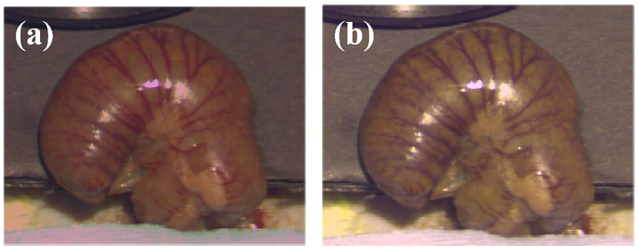

FIGURE 5. Simulated images of rat cecum. (a) Under the STCI. (b) Under the WCPEI.

TABLE 1. Calculated values of α and β.

	STCI	WCPEI
Contrast between tissue and blood vessels, α	6.36×10^{-2}	1.31×10^{-1}
the whiteness condition β	5.45	2.95

Therefore, the calculated WCPEI was expected to enhance blood vessel structures. Moreover, these two peaks were located at short and middle-to-long wavelengths that satisfy the whiteness requirement defined for the WCPEI.

Fig. 5 shows images of rat cecum in which the colors were rendered from a set of hyperspectral image simulations. The original images were captured with a hyperspectral camera, NH-8 (EBA Japan Co., Ltd.). In the first simulation step, the spectral reflectance was calculated pixel-by-pixel based on the hyperspectral images. Next, by multiplying the spectral reflectance by the illuminant spectra and color matching functions, we obtained the tristimulus value, i.e., XYZ. Finally, XYZ was transformed to sRGB via the conversion matrix for display purposes. We note that the reproduction is not exact because the resulting color depends on the display or printer used. However, it is imagined from comparison of these images, the blood vessel structures under the WCPEI can be observed more clearly than those under the STCI. These results suggest that the calculated spectrum can enhance blood vessel structures.

Table 1 shows the calculated values of α and β under each illuminant. This table shows that the WCPEI has a higher contrast than the STCI as it conforms to the whiteness condition $\beta < 3.0$.

B. EVALUATION EXPERIMENT

1) EXPERIMENTAL SETUP

Fig. 6 shows the evaluation experiment setup. The evaluation experiment was conducted subjectively such that observers evaluated the visible blood vessel region under each illuminant condition. We used three rats and set two regions of interest (ROIs) on the surface of each rat cecum. The heat-retention of each rat body and monitoring of the surgical vital signs, i.e., the heart rate and oxygen saturation, were

FIGURE 6. Experimental setup for the evaluation experiment.

conducted during the experiment, as described in III.A. The spectrally-tunable light source was fixed perpendicular to the target areas. Each illuminant intensity was equalized with an illuminance meter, T-10 (Minolta Co., Ltd.). For magnified viewing, observers viewed the target areas through a loupe (O-LIGHT F, Otsuka Optics Co., Ltd.), whose magnification was 200% of the naked eye view.

We evaluated the effectiveness of the illuminants by comparing the ratio of the visible blood vessel region under the two illuminants. Prior to subjective evaluation, a high contrast image was captured with a monochromatic camera (VCXU-23M, Baumer Co., Ltd.) under the LED illuminant with a peak wavelength of 505 nm. Hereinafter, this image is referred to as the 505-nm image. Although this single LED is green and not suitable for routine use, the image taken under this LED presents a remarkable difference between $R_{\mathrm{tis}}(\lambda)$ and $R_{\mathrm{ves}}(\lambda)$.

This 505-nm image was sent to a tablet personal computer (PC). Observers verified the vessel regions on the rat ceca that were visible with the naked eye; subsequently, with a stylus pen, they traced the corresponding blood vessels in the 505-nm image shown on the tablet PC. Meanwhile, the true blood vessel regions in the image were identified manually after subjective evaluation and used as ground truth (GT). Then, we compared the drawn vessel structures and those in the GT.

Five observers per one rat sample evaluated blood vessel structure appearance. Observers were randomly selected for each rat. All observers (age: 22–24 years old, not medical doctors) had normal color vision. They were sufficiently trained to draw a blood vessel region using the tablet PC. For illuminant adaptation, the observers gazed at a white plate under each illuminant for one minute at the point when we changed the illuminant condition. The drawing steps were limited to two minutes for each ROI.

2) EVALUATION METHOD

We quantitatively compared the observed vessel regions and GT vessel regions. Fig. 7 shows the evaluation flow. First, we skeletonized the blood vessel regions in the image.

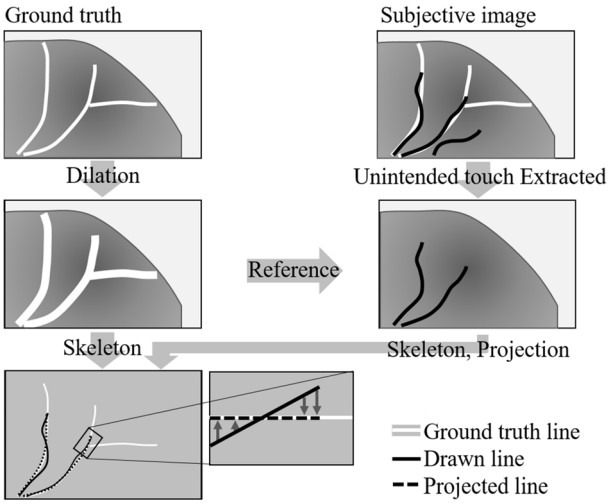

FIGURE 7. Flow of the evaluation experiment.

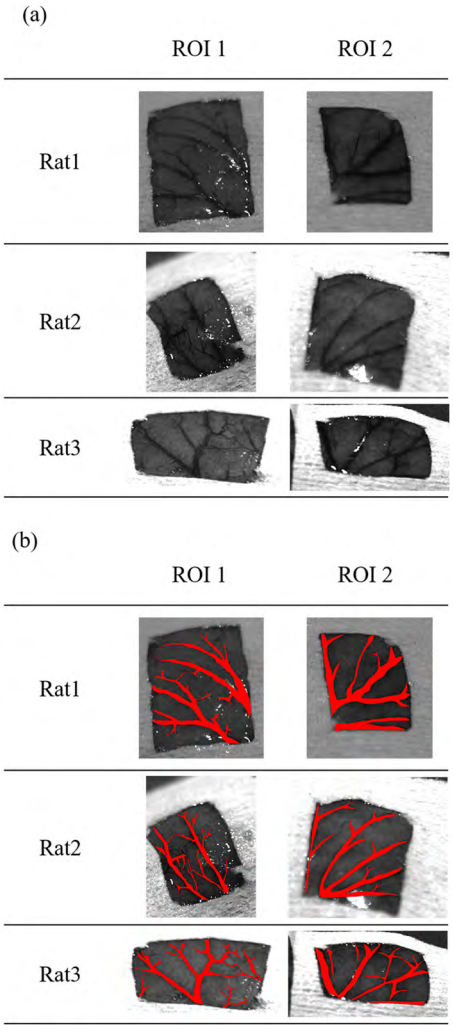

FIGURE 8. Reference images for evaluation experiments. (a) 505-nm images. (b) Ground truth (red regions).

As a preprocessing step, the observed blood vessel region surrounding GT skeleton lines in an observation image was

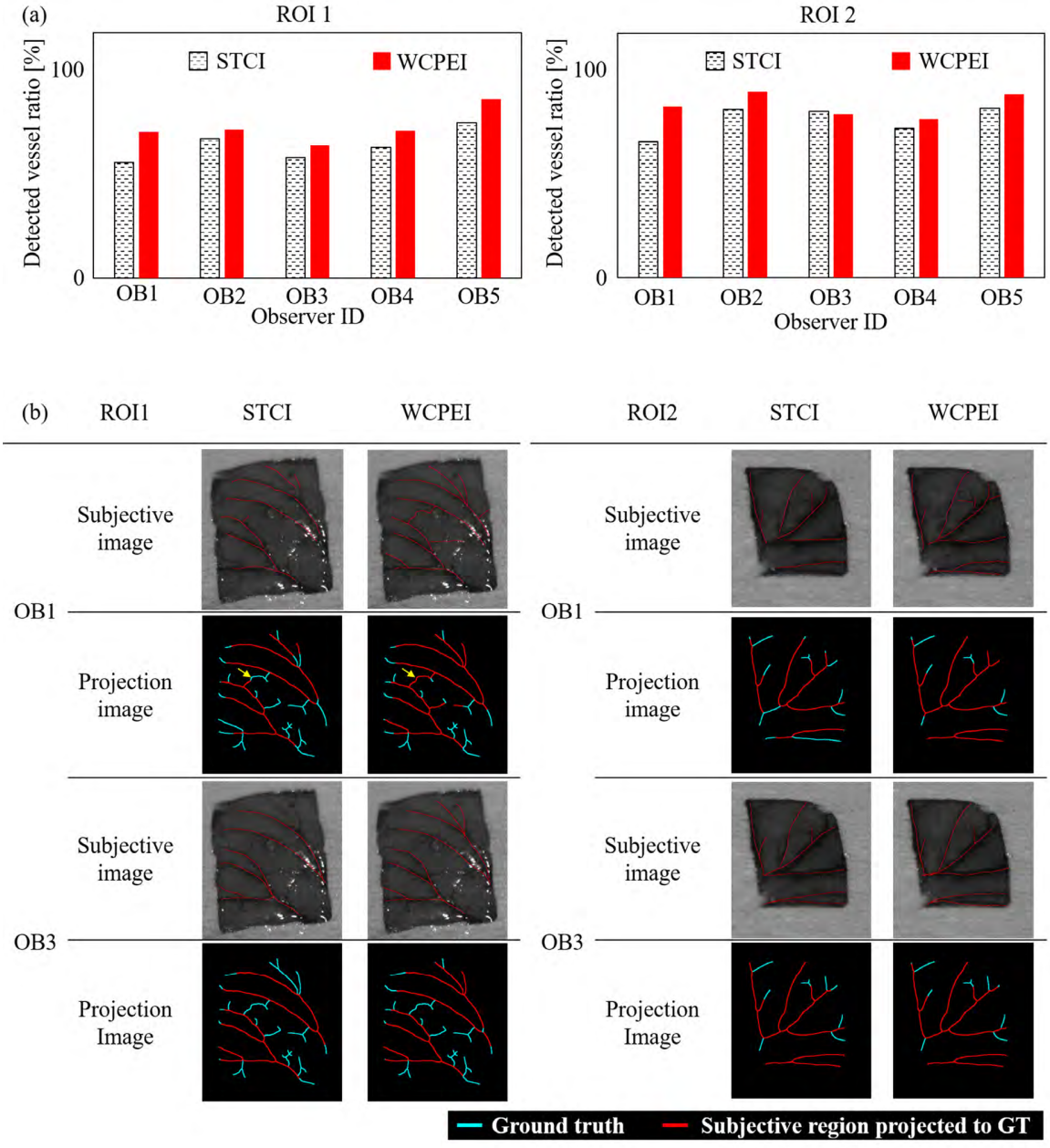

FIGURE 9. Evaluation experiment results for Rat 1. (a) Detected vessel ratio. (b) Subjective and projection images.

extracted to exclude unintended touches that occurred during drawing. The blood vessel region skeleton lines in observation images were extracted and approximated to that of the GT by projection. Finally, we compared the length of the two corresponding lines. As an evaluation index, we calculated the following ratio:

$$C = \frac{\sum l_{subject}}{\sum l_{correct}} \tag{4}$$

where $\sum l_{correct}$ and $\sum l_{subject}$ are the total blood vessel lengths in the GT skeletons and projected lines onto the GT line, respectively. For the statistical evaluation of C between the STCI and the WCPEI, we applied a paired t-test to the C values.

IV. EVALUATION RESULTS AND DISCUSSION

A. THE MOST CONTRAST-ENHANCED IMAGES

Fig. 8(a) shows the 505-nm images for each evaluation and Fig. 8(b) shows the GTs that were prepared manually. We evaluated WCPEI effects using subjective images and vessel-detected ratios.

B. EVALUATION OF EACH ROI

1) RAT 1

Fig. 9(a) shows the detected vessel ratios of rat 1 when exposed to the STCI and the WCPEI. In most cases, the

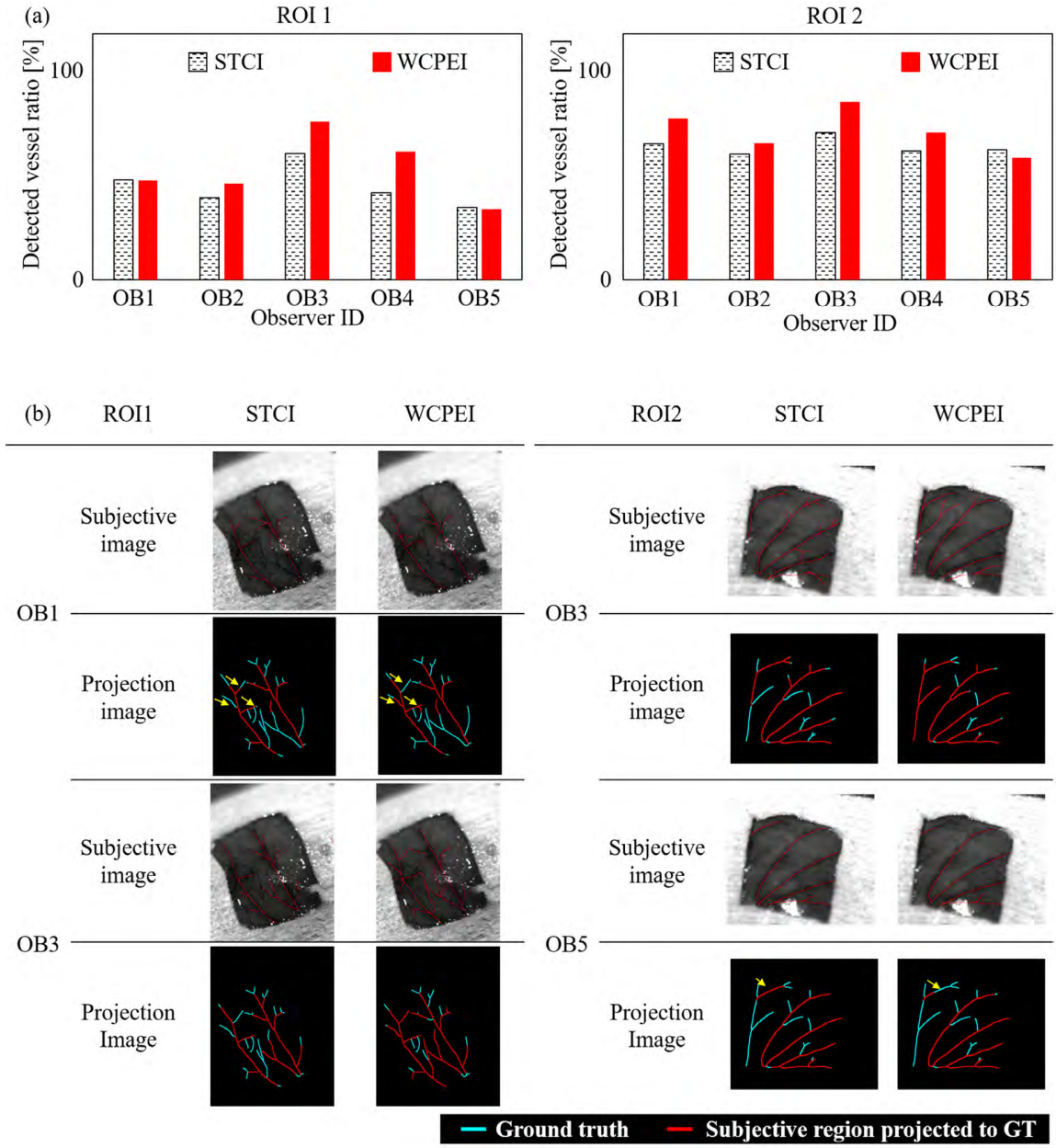

FIGURE 10. Evaluation experiment results for Rat 2. (a) Detected vessel ratio. (b) Subjective and projection images.

C values under the WCPEI were greater than those under the STCI. The paired t-test for the C values indicates that the two illuminants were significantly different (ROI 1: $P = 4.58 \times 10^{-3}$, ROI 2: $P = 3.90 \times 10^{-3}$). Fig. 9(b) shows an example of the subjective vessel region images and projection images. Both image sets under the WCPEI show that the branching vessels were finer than those under the STCI.

2) RAT 2

Fig. 10(a) shows the detected vessel ratios of rat 2. The two illuminants were significantly different (ROI 1: $P = 6.07 \times 10^{-3}$, ROI 2: $P = 4.16 \times 10^{-3}$). In ROI 1, three out of five ratios exhibited greater values under the WCPEI than the STCI. In Fig. 10(b), OB 3 data illustrate an example of this case. Under the WCPEI, thin vessels that surround the center of ROI 1 were observed more clearly than those under the STCI.

Meanwhile, two ratios had similar C values for the two illuminants. In Fig. 10(b), OB 1 data illustrate an example of this case. Entire trends were similar but several thin vessels were detected only under the WCPEI.

For ROI 2, the C values under the WCPEI exceeded those under the STCI (e.g., OB 3) except for one case (OB 5). Fig. 10(b) shows examples for each result. In OB 3, small bifurcations were sensitively detected under the WCPEI. In OB 5, detected regions were generally identical except

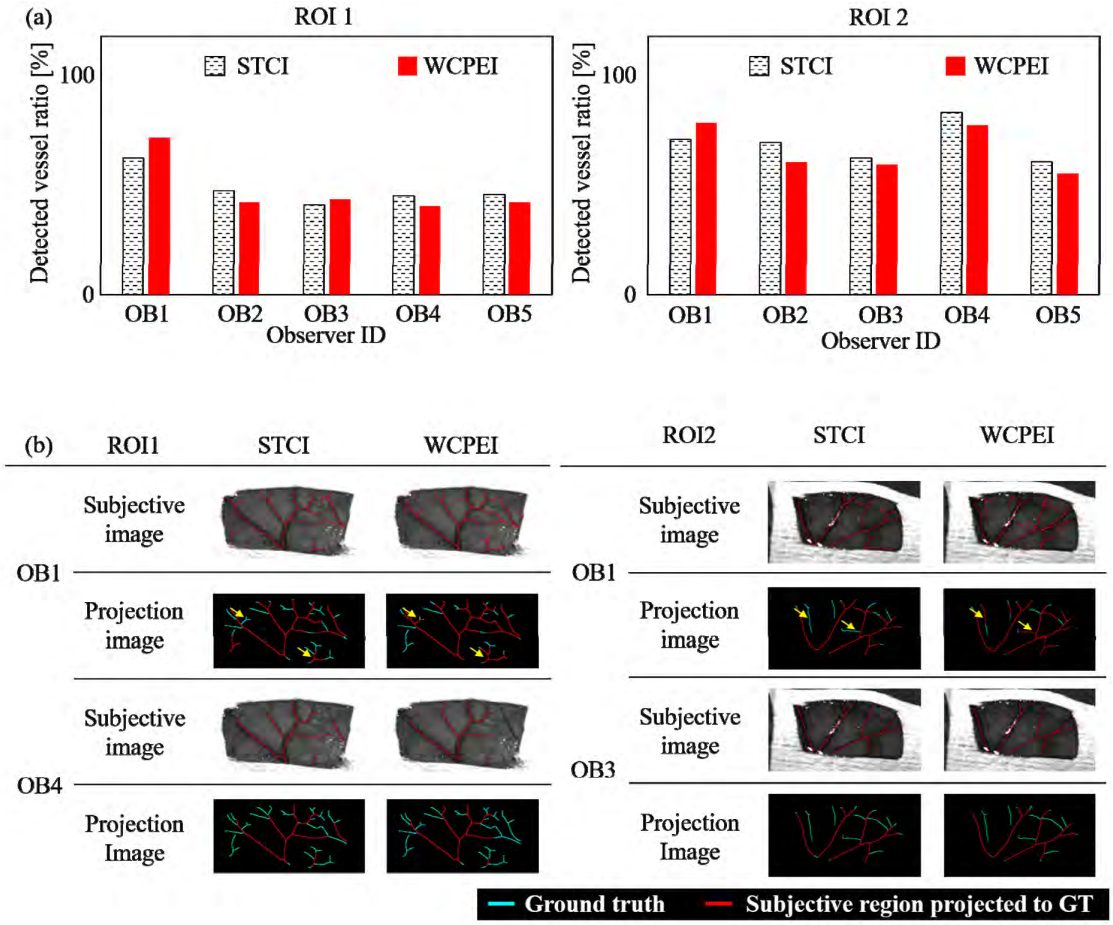

FIGURE 11. Evaluation experiment results for Rat 3. (a) Detected vessel ratio. (b) Subjective and projection images.

for one branch (yellow arrow) for each illuminant condition. In this case, we were only able to observe limited WCPEI effectiveness due to a lack of thin vessels in this ROI.

3) RAT 3

Fig. 11(a) and 11(b) show the detected vessel ratios and several sample images for rat 3, respectively. In ROI 1, there was no significant difference in C values and images between the two illuminant conditions ($P = 4.71 \times 10^{-2}$). This is possibly due to the fact that ROI 1 had fewer thin vessels than other ROIs. For OB 1, several branching vessels were observed more clearly under the WCPEI than those under the STCI (yellow arrow). On the other hand, C value under the WCPEI is less than that under the STCI in OB 4. However, subjective images for OB 4 under the two illuminant conditions are almost the same. Therefore, this tendency may be a consequence of viewing conditions, such as the viewing angle. In ROI 2, there was also no significant difference between the two illuminant conditions $\left(P = 1.71 \times 10^{-2}\right)$. Fig. 11(b) shows the two results for this evaluation. For OB 1, several branching vessels under the WCPEI were more clearly detected than those under the STCI. In contrast, results from OB 3 were nearly identical for each illuminant condition.

C. ENTIRE DATASET EVALUATION

For comprehensive WCPEI evaluation, we applied a paired t-test to the entire dataset. Although variations in P values exist in each ROI, we confirmed significant WCPEI effectiveness for all 30 datasets $\left(P = 7.68 \times 10^{-5}\right)$. Vessel thickness in each ROI appears to mainly cause the variations in P values.

V. CONCLUSIONS

In this study, we proposed an optimization method for a surgical illuminant to enhance blood vessel microstructures on the organ surface. We designed the optimal illuminant spectrum based on the spectral reflectance of the rat cecum. The WCPEI exhibited bimodal peaks located at up to 600 nm, which corresponds to the differences between spectral reflectance in the tissue and blood vessel regions. Then, we conducted subjective evaluation experiments with three rat ceca and confirmed WCPEI effectiveness.

While the WCPEI preserved the color of a white object, it changed the tissue color of the rat ceca. For future studies, we aim to seek a proper balance between tissue-color preservation and blood vessel enhancement. These studies would also require further evaluation experiments and investigations, including subjective evaluation by medical doctors.

REFERENCES

[1] K. Gono, T. Obi, M. Yamaguchi, N. Oyama, H. Machida, Y. Sano, S. Yoshida, T. Hamamoto, and T. Endo, "Appearance of enhanced tissue features in narrow-band endoscopic imaging," *Proc. SPIE*, vol. 9, no. 3, pp. 568–578, May/Jun. 2004.

[2] H.-C. Wang and Y.-T. Chen, "Optimal lighting of RGB LEDs for oral cavity detection," *Opt. Express*, vol. 20, no. 9, pp. 10186–10199, Apr. 2012.

[3] M. Litorja, S. W. Brown, C. Lin, and Y. Ohno, "Illuminants as visualization tool for clinical diagnostics and surgery," *Proc. SPIE*, vol. 7169, pp. 71691B-1–71691B-9, Feb. 2009.

[4] K. Murai, K. Kawahira, and H. Haneishi, "Improving color appearance of organ in surgery by optimally designed LED illuminant," in *Proc. World Congr. Med. Phys. Biomed. Eng.*, vol. 39. Berlin, Germany: Springer, 2013, pp. 1010–1013.

[5] Y.-P. Hsiao, H.-C. Wang, S.-H. Chen, C.-H. Tsai, and J.-H. Yang, "Identified early stage mycosis fungoides from psoriasis and atopic dermatitis using non-invasive color contrast enhancement by LEDs lighting," *Opt. Quantum Electron.*, vol. 47, no. 7, pp. 1599–1611, Sep. 2015.

[6] H.-C. Wang, M.-T. Tsai, and C.-P. Chiang, "Visual perception enhancement for detection of cancerous oral tissue by multi-spectral imaging," *J. Opt.*, vol. 15, no. 5, May 2013, Art. no. 055301.

[7] H. Wang, R. H. Cuijpers, M. R. Luo, I. Heynderickx, and Z. Zheng, "Optimal illumination for local contrast enhancement based on the human visual system," *Proc. SPIE*, vol. 20, no. 1, Jan. 2015, Art. no. 015005.

[8] P. Fält, J. Hiltunen, M. Hauta-Kasari, I. Sorri, V. Kalesnykiene, J. Pietilä, and H. Uusitalo, "Spectral imaging of the human retina and computationally determined optimal illuminants for diabetic retinopathy lesion detection," *J. Imag. Sci. Technol.*, vol. 55, no. 3, pp. 30509-1–30509-10, May 2011.

[9] P. Liu, H. Wang, Y. Zhang, J. Shen, R. Wu, Z. Zheng, H. Li, and X. Liu, "Investigation of self-adaptive LED surgical lighting based on entropy contrast enhancing method," *Opt. Commun.*, vol. 319, pp. 133–140, May 2014.

[10] J. Shen, H. Wang, Y. Wu, A. Li, C. Chen, and Z. Zheng, "Surgical lighting with contrast enhancement based on spectral reflectance comparison and entropy analysis," *Proc. SPIE*, vol. 20, no. 10, Oct. 2015, Art. no. 105012.

[11] P. Bartczak, P. Fält, N. Penttinen, P. Ylitepsa, L. Laaksonen, L. Lensu, M. Hauta-Kasari, and H. Uusitalo, "Spectrally optimal illuminations for diabetic retinopathy detection in retinal imaging," *Opt. Rev.*, vol. 24, no. 2, pp. 105–116, 2017.

[12] Y. Kurabuchi, K. Murai, K. Nakano, T. Ohnishi, T. Nakaguchi, M. Hauta-Kasari, and H. Haneishi, "Optimal design of illuminant for improving intraoperative color appearance of organs," *Artif. Life Robot.*, vol. 24, no. 1, pp. 52–58, May 2019.

[13] M. R. Luo, G. Cui, and C. Li, "Uniform colour spaces based on CIECAM02 colour appearance model," *Color Res. Appl.*, vol. 31, no. 4, pp. 320–330, Jul. 2006.

[14] A. Koschan and M. Abidi, *Digital Color Image Processing*. New York, NY, USA: Wiley, 2008, pp. 11–12.

[15] J. Kennedy, "Particle swarm optimization," in *Encyclopedia of Machine Learning*. New York, NY, USA: Springer, 2010.

[16] G. Wyszecki and W. S. Stiles, *Color Science*, 2nd ed. New York, NY, USA: Wiley, 1982.

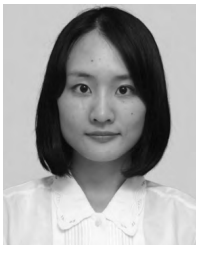

YOKO KURABUCHI received the B.E. and M.E. degrees from Chiba University, Chiba, Japan, in 2016 and 2018, respectively, where she is currently pursuing the Ph.D. degree with the Graduate School of Science and Engineering. Her current research interests include the medical imaging and optics.

KAZUYA NAKANO received the M.S. and Ph.D. degrees from the Tokyo Institute of Technology, in 2007 and 2013, respectively. He was with the Mizuho Information & Research Institute (MHIR), from 2007 to 2009. He was an Assistant Professor with Nippon Sport Science University, from 2013 to 2014 and the Tokyo University of Science, from 2015 to 2016. Since 2017, he has been a specially appointed Assistant Professor with the Center for Frontier Medical Engineering, Chiba University. His current research interests include diffuse reflectance spectroscopy, optical security, information photonics, and applied physics.

TAKASHI OHNISHI received the M.S. and Ph.D. degrees from Chiba University, in 2010 and 2013, respectively, where he is currently an Assistant Professor with the Center for Frontier Medical Engineering, Chiba University. His current research interests include image processing, image registration, and pathological images.

TOSHIYA NAKAGUCHI received the B.E., M.E., and Ph.D. degrees from Sophia University, Tokyo, Japan, in 1998, 2000, and 2003, respectively. He was a Research Fellow supported by the Japan Society for the Promotion of Science, from 2001 to 2003. He joined the Department of Information and Image Sciences, Chiba University, as an Assistant Professor, in 2003. He has been a Professor of the Center for Frontier Medical Engineering (CFME), since 2016. He has been a Visiting Professor of Zhengzhou University.

MARKKU HAUTA-KASARI received the M.S. degree in computer science from the University of Kuopio, Finland, in 1994, and the Ph.D. degree in information processing from the Lappeenranta University of Technology, Finland, in 1999. He is currently a Professor in computer science with the University of Eastern Finland. He is also the Head of the Spectral Color Research Group. His research interests include spectral color research, pattern recognition, and computer vision.

HIDEAKI HANEISHI received the M.S. and Ph.D. degrees from the Tokyo Institute of Technology, in 1987 and 1990, respectively. He joined Chiba University as a Research Associate, in 1990. He was a Visiting Research Scientist with the Department of Radiology, University of Arizona, from 1995 to 1996. He has been a Full Professor of the Center for Frontier Medical Engineering (CFME), since 2007. He is also the Director of CFME.